Lattices with internal resonator defects

S. Hauver,[1] X. He,[2] D. Mei,[1] E. G. Charalampidis,[1] P. G. Kevrekidis,[1] E. Kim,[3,4,5] J. Yang,[3] and A. Vainchtein[6]
[1]*Department of Mathematics and Statistics, University of Massachusetts, Amherst, Massachusetts 01003-4515, USA*
[2]*Department of Electrical and Computer Engineering, University of Massachusetts, Amherst, Massachusetts 01003-4515, USA*
[3]*Department of Aeronautics and Astronautics, University of Washington, Seattle, Washington 98195-2400, USA*
[4]*Division of Mechanical System Engineering, Chonbuk National University, Jeonju-si, Jellabuk-do 54896, Republic of Korea*
[5]*Automotive Hi-Technology Research Center & LANL-CBNU Engineering Institute Korea, Chonbuk National University, Jeonju-si, Jellabuk-do 54896, Republic of Korea*
[6]*Department of Mathematics, University of Pittsburgh, Pittsburgh, Pennsylvania 15260, USA*

(Received 12 April 2018; published 11 September 2018)

We consider a variety of settings involving chains with one or more defects stemming from the introduction of nodes bearing internal resonators. Motivated by experimental results in woodpile elastic lattices with one or two defects, we consider a variety of different theoretical scenarios. These include multidefect chains and their ability to transmit, reflect, and especially trap energy. Moreover, they involve defects which are spatially separated and either statically or, more effectively, dynamically enable the confinement of energy between the separated defects. Wherever possible, comparisons of the experiments with numerical simulations as well as with theoretical intuition are also offered, to provide a justification for the observed findings.

DOI: 10.1103/PhysRevE.98.032902

I. INTRODUCTION

The study of granular crystals and of related topics has received considerable attention especially over the last decade. To a considerable extent this is arguably due to the significant experimental progress that has complemented theoretical and numerical investigations; see, e.g., [1–4] for earlier and [5–7] for recent reviews. In these media with extensively tunable properties, traveling waves have been of particular interest. More recently numerous other excitations have been examined including, but not limited to, defect modes, bright and dark breathers, and shock waves [5,7]. At the same time, a diverse host of applications including, e.g., actuating devices [8], acoustic lenses [9], mechanical diodes [10–12], logic gates [13], and sound scramblers [14,15] has also been proposed, adding a more practical dimension to the theoretical appeal of the subject.

A twist on this theme of granular crystals that has led to numerous recent studies concerns the subject of the so-called locally resonant granular crystals, otherwise known as mass-in-mass (MiM) or mass-with-mass (MwM) systems. The MiM and MwM systems have already been experimentally realized in [16] and [17], respectively. These realizations were chiefly linear, due to externally imposed static precompression of the chain, and geared towards the remarkable metamaterial-type properties that these systems possess. A prototype of a strongly nonlinear granular chain with a single MwM defect was also demonstrated in [18], where numerical investigations of the system, complemented by multiscale asymptotic analysis of a reduced model, demonstrated an ability of such defect to trap and reflect portions of the energy carried by a solitary wave. More recently, a different type of experiment was realized showcasing highly nonlinear propagation in a locally resonant granular system [19]. In particular, this experiment featured a so-called woodpile configuration consisting of orthogonally stacked rods [20] and demonstrated that the bending vibrations of the rods can play the role of the local resonator within the chain. It was also shown that depending on the properties of the system (i.e., the length of the rods), one can controllably incorporate one or more such resonators and observe unique types of wave forms not previously explored in granular chains, including weakly nonlocal solitary waves.

In the present work, we consider a strongly nonlinear granular chain with a finite number of MwM defects, focusing particularly on the cases of adjacent and separated defects that were only briefly explored in [18]. This setting interpolates between the single-defect case that was the main focus of [18] and the case of a woodpile lattice of [19,20], where each granule is effectively coupled to a local resonator. To motivate this work, we begin by presenting experimental results for woodpile lattices involving one and two defects represented by longer rods. These experiments allow us to infer the fraction of transmitted, reflected, as well as trapped kinetic energy for each case, in very good agreement with the corresponding simulation results. In light of these experimental possibilities, we theoretically explore a number of variants of the problem. More specifically, we consider a "defective" region of variable domain and examine how the different energy fractions scale with the size of this region. We then explore the possibility of separating the two defects, and also of using such a separation to attempt to induce (possibly also dynamically) a trapping of the traveling solitary wave between the two defects. We offer detailed comparisons of our experimental results with corresponding numerical simulations, as well as, wherever possible, of the numerical computations with theoretical considerations.

Our presentation is structured as follows. In Sec. II, we introduce our woodpile experimental setup and the mathematical model describing it and then give an overview of the experimental results and their comparison to numerical

computations. In Secs. III (for single or adjacent defects) and IV (for more general, and also dynamically variable in time, settings) we explore a number of scenarios (as discussed above) via direct numerical simulations and corresponding theoretical analysis. Finally, in Sec. V, we summarize our findings and present our conclusions.

II. EXPERIMENTS USING SIMPLE 1D WOODPILE LATTICES AND THE THEORETICAL MODEL

Over the last few years, there have been several experimental studies of granular chains coupled with localized linear oscillators (internal resonators) at one or more defect sites. In a recent work [16], a system of this type was constructed using a chain of hollow spheres that embed resonators by using polymeric holders. While this system demonstrated the feasibility of developing tunable frequency band gaps, it is susceptible to damping due to the viscoelastic nature of the polymeric holders. Another complex system, with a ring resonator attached to the defect bead, has been reported in [17]. Some of the present authors built a one-dimensional (1D) woodpile lattice system [20], which derives the local resonances of constituents from the bending vibrations of longitudinal woodpile elements. Using this setup, we have successfully verified the versatile propagation of nonlinear waves, which transmit, modulate, or attenuate depending on the interplay between the propagating nonlinear waves and the local resonances of woodpile components [19]. This also led to the experimental verification of highly nonlinear weakly nonlocal waves (often referred to as nanoptera) in the setting of homogeneous 1D woodpile lattice systems. In the present study, we employ such woodpile systems to validate simple representative cases of the lattice with one or more internal resonator defects, while using numerical simulations for corresponding parametric studies.

A. Experimental setup and theoretical model

We built a test setup as shown in Fig. 1 to experimentally demonstrate the propagation of solitary waves in a woodpile lattice and their interactions with a defect (i.e., a node bearing a local resonator). In this setup, we consider a chain of 40 orthogonally stacked cylindrical rods. Each rod is made of fused quartz (Young's modulus $E = 72$ GPa, Poisson's ratio $\nu = 0.17$, and density $\rho = 2200$ kg/m^3) and has the radius $R = 2.5$ mm. All cylinders have length 20 mm, except for a single "defect" rod in the middle, which is 40 mm long. To excite solitary wave propagation in the woodpile lattice, we apply an impact on the top of the chain by dropping a 10-mm-diameter glass sphere from a 20-cm drop height with impact velocity of $V = 1.98$ m/s. A soft foam is located at the bottom of the chain to suppress and delay the wave reflection from the boundary.

To observe the wave propagation in the chain we use a laser Doppler vibrometer (LDV) mounted on an automatic guiding rail. When the striker impacts on the top rod, the piezoelectric sensor bonded on the surface of the top rod generates voltage, which in turn triggers the LDV and measures a particle's velocity. We record the particles' velocity profiles one by one in each impact event and synchronize all collected signals

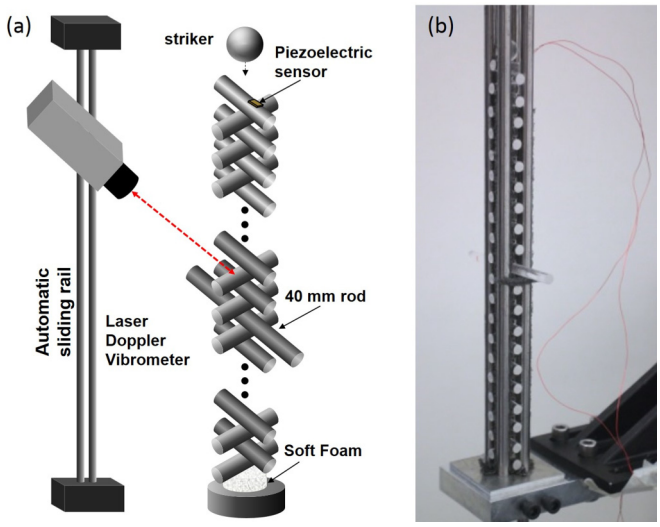

FIG. 1. (a) Illustration of experimental setup involving the woodpile chain, the striker leading to the formation of the wave and the laser Doppler vibrometer enabling its probing. (b) Digital image of the woodpile chain with a single-defect rod. The horizontal posture of the rods is supported by soft polyurethane foam inserted between the rods. The effect of the foam on wave propagation is negligible due to the orders-of-magnitude lower stiffness of the foam compared to the quartz cylinders [19].

with respect to the trigger signals. This enables us to visualize the wave propagation in space-time velocity evolution plots presented in the next subsection.

The vibrations of cylindrical elements in the woodpile lattice play a role of local resonances. The bending vibration modes are particularly important, since they carry most of the vibration energy in the frequency domain of our interest (below 50 kHz). The slender cylindrical rods develop low-frequency bending modes, and our previous study showed that they can be coupled with the propagating nonlinear waves [19]. The mode coupling mechanism depends on the resonant frequency of the bending mode, and if the resonant frequency is too high compared to the characteristic time of the propagating nonlinear waves, the coupling effect becomes weak. We find that the first bending modes of the 20- and 40-mm rods are approximately 55.2 and 15.2 kHz, respectively, based on our previous numerical and experimental investigations [19,20]. At an impact excitation, the chain composed of 20-mm rods without defect shows single-side weakly nonlocal (nanopteronic) solitary waves, which consist of a leading solitary wave and an oscillating tail behind it [19]. Since the mechanical energy contained in this wave tail is negligibly small compared to that of the solitary wave, we can safely neglect the effect of the wave tail in the present considerations. However, the first bending mode of the 40-mm rod is low enough to be strongly coupled with the propagating solitary wave. We model its oscillating behavior by a secondary mass m attached to the primary element of mass M in a homogeneous granular chain via a linear spring of stiffness K. We thus obtain an effective description of our experimental setup as a granular system with a single MwM defect [18]

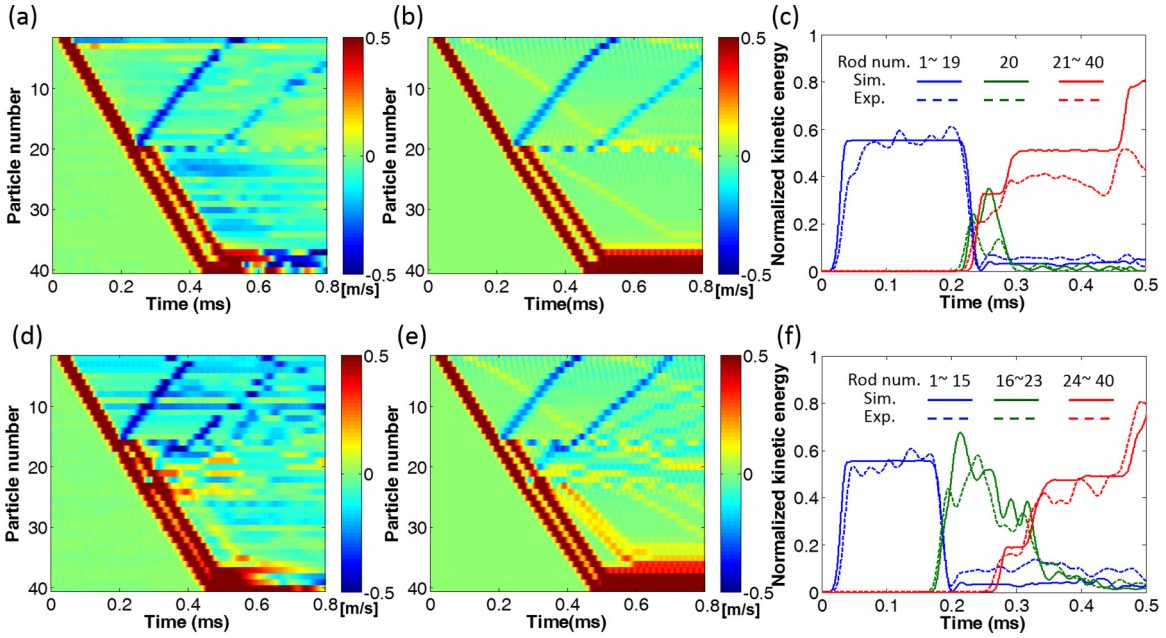

FIG. 2. Solitary wave propagation in the woodpile chain with a single defect (panels (a)–(c)) and two separated defects (panels (d)–(f)) in experiments and numerical simulations. See the main text for details. Panels (a) and (d) show space-time velocity evolution plots obtained from experiments with one and two defects, respectively, and panels (b) and (e) show the corresponding results of the numerical simulations. Panels (c) and (f) compare experimental and numerical evolution of the normalized kinetic energy fraction in the chain with a single and double defect rods, respectively.

governed by

$$M\ddot{u}_n = a\left([u_{n-1}-u_n]_+^{3/2} - [u_n - u_{n+1}]_+^{3/2}\right) - K(u_i - v_i)\delta_{ni}, \quad n = 1, \ldots, N_r,$$
$$m\ddot{v}_i = K(u_i - v_i), \tag{1}$$

where $N_r = 40$ is the number of rods, $i = 20$ is the position of the defect rod, and δ_{ni} is the Kronecker delta, i.e., $\delta_{ni} = 1$ when $n = i$ and zero otherwise. The displacement of nth primary mass at time t is denoted by $u_n(t)$, with $\ddot{u}_n(t) = d^2u_n(t)/dt^2$, while the displacement of the secondary mass coupled to the ith element is $v_i(t)$. The rods interact via Hertzian contact forces characterized by the exponent of 3/2 and constant $a = (2E\sqrt{R})/[3(1-\nu^2)] = 2.47 \times 10^9$ N/m$^{3/2}$. The tensionless character is indicated by the subscript +, which means that the corresponding term is nonzero only when the quantity in the parentheses is positive. Using the approach described in [19,20], one finds the effective parameters $M = 0.838$ g, $m = 0.894$ g, and $K = 3961$ kN/m for our experimental setup. Here the primary mass M is close to the mass of the 20-mm rod (0.866 g).

The impact applied to the first (top) rod of the chain by a striker with velocity V is modeled by the initial conditions

$$u_n(0) = v_i(0) = 0, \quad \dot{u}_n(0) = \dot{v}_i(0) = 0 \quad \text{for } n \neq 1,$$
$$\dot{u}_1(0) = V. \tag{2}$$

B. Experimental and numerical results for single and double MwM defects

We conduct preliminary testing on simple chains containing single and double impurities bearing local resonators in an otherwise homogeneous chain. Figure 2(a) shows space-time velocity plots in the chain containing, as described above, a single defect rod (40-mm rod) at the center of the chain (20th particle's position from the top of the chain). The corresponding numerical results for the discrete element model are shown in Fig. 2(b). Here we use a fourth-order Runge-Kutta method to solve Eq. (1) with initial conditions (2). We use free boundary conditions at both ends of the chain, which is reasonable in the time span that we are interested in. Note that the wave reflection at the boundary does not affect the dynamics in this time frame, as shown in Fig. 2.

An impact excitation generates multiple solitary waves due to the larger inertia of the striker compared to the mass of the 20-mm rod. However, the secondary solitary wave is negligibly small compared to the primary one, so it is not captured in the experiment. The propagating primary solitary wave experiences scattering at the defect rod and splits into multiple wave packets. A part of the energy is reflected back at the defect site due to the larger effective mass of the defect rod (40-mm rod) than that of 20-mm rod. We also observe that a portion of the energy is transferred through the defect rod in the form of solitary waves without noticeable time delay. Interestingly, a fraction of the incident energy is stored in the defect rod, and much of it is released after a time delay. Therefore a strong secondary solitary wave is generated just behind the primary transmitted wave. The rest of the energy is trapped in the defect rod in the form of local oscillations, which slowly disperse to the neighboring rods. Kinetic energy profiles obtained from the experiment and numerical simulations are presented in Fig. 2(c), where the energy is normalized with respect to the impact energy. Here, temporal energy profiles are represented by three different

regions (ahead of the defect rod, at the defect rod, and behind the defect rod), enabling us to quantitatively compare the energy transmission, reflection, and the energy trapped in the defect rod. In this model, most kinetic energy is transmitted, while about 0.4% and 2.0% of the total kinetic energy are trapped and reflected at the defect site, respectively. However, it is worth noting that the kinetic energy in total is not a conserved quantity, hence these fractions are, in principle, time dependent. Here we only compare kinetic energy instead of total energy because it is difficult to measure potential energy accurately using the current measurement technique. That is, we measure particles' velocities using LDV, and the calculation of particles' relative displacements based on velocity data is susceptible to integration errors. Nevertheless, in the numerical considerations that follow, we will use instead the total energy of the system in order to offer a more theoretically well-founded basis, given the conservation of the total energy, for the consideration of energy transmission, reflection, and trapping.

Figures 2(d) and 2(e) show experimental and numerical profiles of wave propagation, respectively, when there are two defects (at the 16th and 23rd particle positions from the top of the chain) separated by seven particles in the chain. The corresponding normalized kinetic energy profiles are shown in Fig. 2(f). In this case, multiple scattering events appear to arise in each of the defect rods and more energy is reflected (about 4%) and trapped between the two defects (about 2%) in a long time.

III. FURTHER NUMERICAL FINDINGS

In the previous section, we employed the 1D woodpile system to realize a lattice with internal resonator defects and successfully demonstrated the feasibility of trapping mechanical energy in the simple cases of single and double defects. While this setup provides its own advantages, we also note that it has limitations, particularly in manipulating system parameters (e.g., mass and stiffness) independently. For example, if we change the length of the defect rod, its resonant frequency will change, and this will in turn cause the rearrangement of the effective secondary mass and stiffness parameters for the defect rod. Thus, in what follows, we resort to numerical simulations to fully investigate various scenarios of local defects in the system.

We first look at a more systematic exploration of the possibility of having more than one defect of the resonator type. It is convenient to write the governing equations in the dimensionless form, using $(MV^2/a)^{2/5}$ as the length scale and $(MV^2/a)^{2/5}/V$ as the time scale, where we recall that M is the primary mass, a is the Hertz constant, and $V > 0$ is the impact velocity. This yields two dimensionless parameters: the ratio of the two masses,

$$\epsilon = \frac{m}{M}, \tag{3}$$

and the strength of the linear coupling measured by $\kappa = K/(M^{1/5}a^{4/5}V^{2/5})$. In the experimental setup presented in Sec. II we had $\epsilon \simeq 1.0$ and $\kappa \simeq 0.07$. The dimensionless equations governing the system with $L+1$ adjacent defects are

$$\begin{aligned} \ddot{u}_n &= [u_{n-1}-u_n]_+^{3/2} - [u_n - u_{n+1}]_+^{3/2} - \sum_{j=0}^{L} \kappa(u_j - v_j)\delta_{nj}, \\ \epsilon\ddot{v}_j &= \kappa(u_j - v_j), \quad j = 0,\dots,L, \quad n = -N,\dots,N. \end{aligned} \tag{4}$$

The first defect is placed in the middle of the chain at $n = 0$, with n ranging from $-N$ to N here and in what follows. The corresponding velocity-impact initial conditions are

$$\begin{aligned} &u_n(0) = v_0(0) = 0, \quad \dot{u}_n(0) = \dot{v}_0(0) = 0 \quad \text{for } n \neq n_S, \\ &\dot{u}_{n_S}(0) = 1, \end{aligned} \tag{5}$$

where the initially excited n_Sth site above the defect ($n_S < 0$) has unit impact velocity.

An important diagnostic quantity of the conservative system under consideration is the total energy

$$E = \sum_{n=-N}^{N} e_n, \tag{6}$$

where e_n stands for the energy density given by

$$\begin{aligned} e_n = \frac{1}{2}\dot{u}_n^2 + \frac{1}{2}\sum_{j=0}^{L}\left[\epsilon\dot{v}_j^2 + \kappa(u_j - v_j)^2\right]\delta_{nj} \\ + \frac{1}{5}\left\{[u_{n-1}-u_n]_+^{5/2} + [u_n - u_{n+1}]_+^{5/2}\right\}. \end{aligned} \tag{7}$$

This will also enable us to characterize the fractions of the energy that will be reflected (R) and transmitted (T) from as well as trapped ($E_{\rm tr}$) inside the "defective" region, and how these fractions are affected by the number $L+1$ of the adjacent defects. The corresponding fractions of the energy can be defined as follows:

$$R = \frac{1}{E}\sum_{n=-N}^{-2} e_n, \quad T = \frac{1}{E}\sum_{n=L+2}^{N} e_n, \quad E_{\rm tr} = 1 - T - R, \tag{8}$$

where we have (admittedly, with some degree of arbitrariness) assumed that the trapping region encompasses the defect sites and the particles adjacent to the first and last defects, while energy fractions to the left and right of that represent, respectively, the reflected and transmitted contributions to the energy. Note that, contrary to the experimental setup, which can more accurately capture the velocities and hence the kinetic energy, here we use as a more adequate diagnostic (due to its total conservation) the full energy of the system.

Using a fourth-order Runge-Kutta method, we numerically integrated Eq. (4) forward in time with $N = 100$ and $0 \leqslant L \leqslant 9$, with zero boundary conditions and initial conditions (5) with $n_S = -25$. Figure 3 displays the space-time evolution of velocities for $\epsilon = 10$ and $\kappa = 1$, with left and right panels corresponding to $L = 2$ and $L = 6$, respectively.

Figure 4 shows how the reflected, transmitted, and trapped fractions of the energy defined in (8) vary as functions of the mass ϵ of the defect for the cases of 1, 3, 6, and 7 resonators composing the relevant "defective region" within the chain for $\kappa = 1$. We remark that we vary ϵ, while keeping $\kappa = 1$ fixed, since the latter prefactor can be absorbed in a rescaling of the

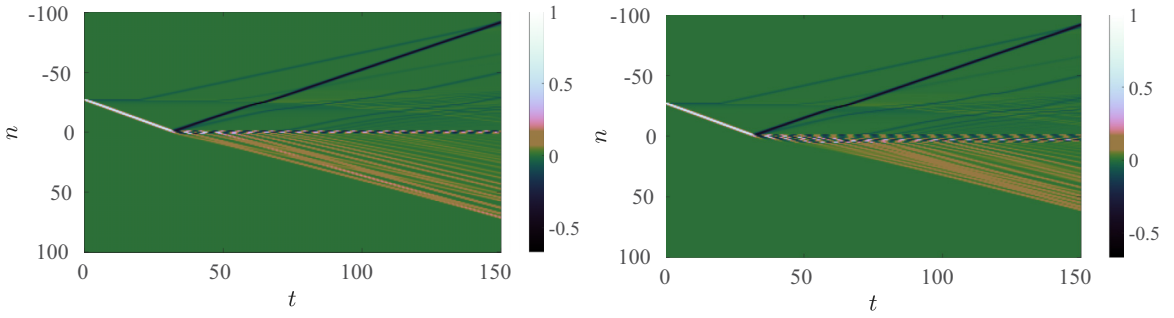

FIG. 3. Space-time evolution of velocities in numerical simulations with $\epsilon = 10$, $\kappa = 1$ and defect lengths 3 ($L = 2$, left panel) and 7 ($L = 6$, right panel). In the second case the two edge defects are visibly more separated demonstrating a wider defect zone.

amplitude of u_n and time. To obtain the parametric variation results shown in the figure, we increase ϵ by $\Delta\epsilon = 0.1$ and evaluate the energy fractions long after the interaction of the incoming wave with the defect (i.e., the time integration is performed for $t \in [0, 150]$).

In all panels, as $\epsilon \to 0$, physically corresponding to the case where the resonators are essentially absent from the system, we have almost perfect transmission of the energy which is observed for all L. However, the cases with multiple adjacent defects are different from the single-defect case for large values of ϵ. Generally, when $\epsilon \gg 1$, there is almost no transmitted energy, while there is a large amount of reflected energy. Importantly for our considerations involving the question of how much energy can be trapped in the resonator region, we see a significant increase (as well as, arguably, a more complicated functional dependence) of this fraction on ϵ as the number of resonators increases. We examine as diagnostics both the global maximum of this trapped fraction, as well as the ϵ for which it occurs. This is shown in detail in Fig. 5, presenting the relevant (global) maximum for $\epsilon \in (0, 60]$. Despite the somewhat nonsmooth nature of the relevant graph, overall the trend is apparent and illustrates a monotonic, concave down dependence of the associated fraction of the energy on the length of the relevant region within the chain.

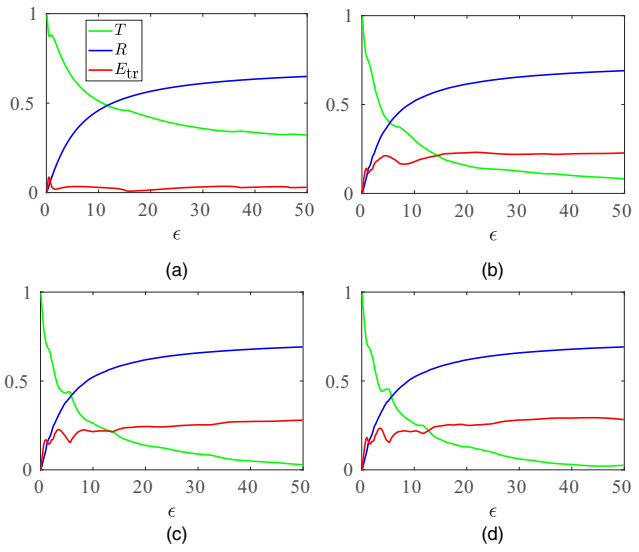

FIG. 4. The reflected (R), transmitted (T), and trapped ($E_{\rm tr}$) energy fractions as functions of the mass ϵ with $\kappa = 1$ for the cases of (a) single defect ($L = 0$), (b) three adjacent defects ($L = 2$), (c) six adjacent defects ($L = 5$), and (d) seven adjacent defects ($L = 6$).

IV. SEPARATING THE DEFECTS: FORMING AN ENERGY-TRAPPING REGION

Going back to the linear coupling setting, we now consider another important case when two defects are placed at a certain number of beads apart. This represents a generalization of the problem with adjacent defects discussed above. The goal in this case is to be able to trap, to the degree possible, the energy of a propagating wave between the two defect sites, $n = d_1$ and $n = d_2$, at which the primary unit (upon rescaling) masses are coupled to secondary masses ϵ_1 and ϵ_2 with displacements v_{d_1} and v_{d_2}, respectively, and, for simplicity, the same coupling parameter κ. Our trapped energy ($E_{\rm tr} = 1 - T - R$) maximization then leads us to seek maximizing the quantity

$$E_{\rm tr} = \frac{1}{E}\sum_{n=d_1-1}^{d_2+1} e_n, \tag{9}$$

where the energy density e_n in this case is given by

$$e_n = \frac{1}{2}\dot{u}_n^2 + \frac{1}{2}\sum_{j=1}^{2}\left[\epsilon_j \dot{v}_{d_j}^2 + \kappa\left(u_{d_j} - v_{d_j}\right)^2\right]\delta_{nd_j} + \frac{1}{5}\left\{[u_{n-1} - u_n]_+^{5/2} + [u_n - u_{n+1}]_+^{5/2}\right\}, \tag{10}$$

and E is the total energy.

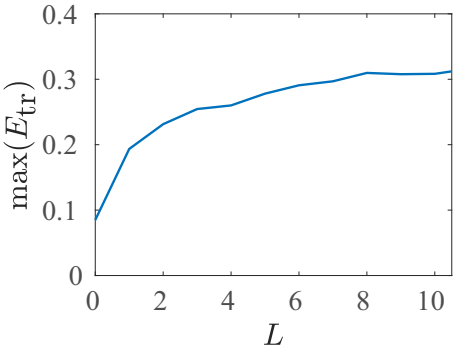

FIG. 5. The global maximum (over the mass of the resonator ϵ) of the trapped energy as a function of the length L of the "defective" region (bearing the resonators), with $\kappa = 1$.

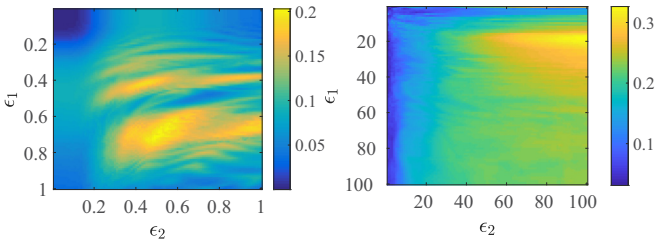

FIG. 6. Contour plot of the trapped energy for various ϵ_1 and ϵ_2 ratios, as a two-dimensional function of both variables (for fixed $\kappa = 1$). The left panel is for a finer grid spacing and smaller yet important (in terms of energy trapping) region of the two-dimensional parameter space, while the right panel represents a coarser but extended grid. The left panel shows the domain $[0.1, 1]^2$ with an ϵ increment of $\Delta\epsilon = 0.01$ and the right panel shows the domain $[1, 100]^2$ with a $\Delta\epsilon = 1$.

As a representative example, we consider the wide region between the two defects, with $d_1 = 0$, and $d_2 = 20$. Running the same simulations as above, we vary the masses ϵ_1 and ϵ_2 of the defects and measure the trapped energy as shown in Fig. 6. The left panel of the figure corresponds to a smaller mass ratio domain, $\epsilon_1 \times \epsilon_2 = [0.1, 1]^2$, whereas the right panel corresponds to a larger domain, $\epsilon_1 \times \epsilon_2 = [1, 100]^2$. For the smaller domain we increment $\epsilon_{1,2}$ by $\Delta\epsilon = 0.01$, and for the larger domain we have $\Delta\epsilon = 1$. The maximum of the trapped energy fraction for the larger domain with the coarser grid (see the figure caption for details) arises when $\epsilon_1 = 13$ and $\epsilon_2 = 100$ with $E_{\text{tr}} = 0.3926$, i.e., a significant component of the energy being trapped in the relevant region. Importantly, note that in this case the optimum arises on the "boundary" of the parametric domain associated with the maximal mass of the second defect, enabling (presumably) the largest possible (inward) reflection from that boundary. In the case of the smaller domain with finer mesh it occurs when $\epsilon_1 = 0.67$ and $\epsilon_2 = 0.54$ with $E_{\text{tr}} = 0.2112$. These cases are illustrated in Fig. 7. On the finer mass ratio scale (left panel), the main contribution to the trapped energy stems from the pair of defect beads which interact with their respective resonator masses in such a way as to contain a substantial fraction of the solitary wave as it crosses the defect. This is somewhat in contrast to the coarser ϵ case, in which the primary contributor to the trapped energy is the solitary wave itself, bouncing between the two defects and resulting in a significant fraction of the energy being confined in the region between the defects.

Returning to our main goal, we would like to attempt to quantify the mechanism behind these optimal parameters for trapping the energy in the region between the defects. As a crude approximation, we assume for the present consideration that energy trapped at the resonator defect sites is negligible (an assumption partially justified by the limited ability of each individual defect to trap the energy) and only consider the transmitted and reflected fractions of the energy from the two defects as follows:

$$E_{\text{tr}}(\epsilon_1, \epsilon_2) = T_1(\epsilon_1)R_1(\epsilon_2)R_2(\epsilon_1)R_3(\epsilon_2). \tag{11}$$

The implicit assumption here is that the energy trapped in the region of interest results from a series of "favorable" interactions with the defects, i.e., an initial transmission from the first defect, followed by a reflection from the second and then further reflections from both defects [of which we have only included the first pair in Eq. (11)]. We first consider the case of equal-mass defects, $\epsilon_1 = \epsilon_2 = \epsilon$, where T_1, R_1, R_2, and R_3 are determined in a fitted form from the data obtained in the top left panel of Fig. 4. This yields, as a reasonable approximation,

$$\begin{aligned} T_1(\epsilon) &= 0.5630\epsilon^{-0.0110} + 0.3345, \\ R_1(\epsilon) = R_2(\epsilon) = R_3(\epsilon) &= 0.5491\tanh(0.0830\epsilon) + 0.0760, \end{aligned} \tag{12}$$

where both lines were fitted with a relative error $\approx$0.0369. The plot of $E_{\text{tr}}(\epsilon)$ versus the actual, numerically computed trapped energy is shown in the left panel of Fig. 8 with solid black and red lines, respectively. The approximation has the right qualitative trend (especially given our crude assumptions) for the coarser regime of larger values of ϵ but breaks down as $\epsilon \to 0$. One reason for this discrepancy could be the fact that we considered the T and R (individual) fits based on the coarser ϵ scale. Moreover, the dynamics of smaller chunks of energy (detached upon collisional events with the defects from the primary solitary wave) is not adequately captured within this approximation.

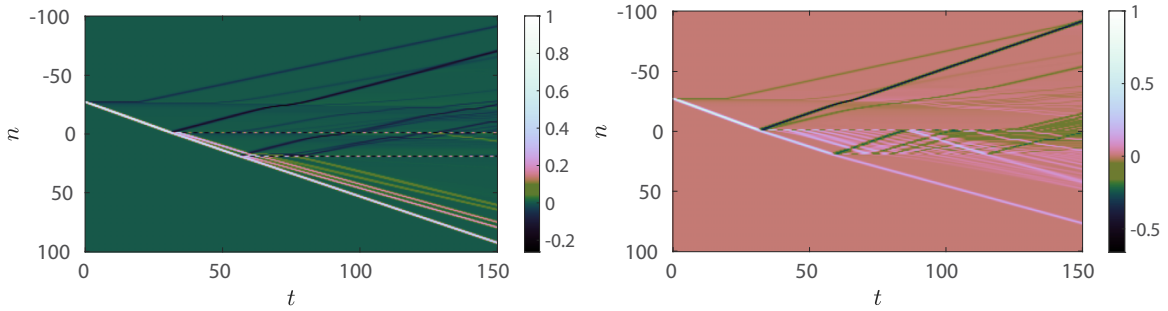

FIG. 7. Space-time velocity plot for the (ϵ_1, ϵ_2) combinations that yield the maximal trapping. The left panel corresponds to the (ordered) pair $(\epsilon_1, \epsilon_2) = (0.67, 0.54)$, and the right panel to $(\epsilon_1, \epsilon_2) = (13, 100)$. In the left panel we see that the major contributor to the trapped energy is the energy emanating from the resonator nodes, as opposed to the right panel where we see that the major contributor to the trapped energy is the motion of a single solitary wave bouncing back and forth between the beads. In addition, in the right panel we can also discern slightly smaller solitary waves emanating from the ringing vibrations of the two defects, as indicated by the faint blue lines.

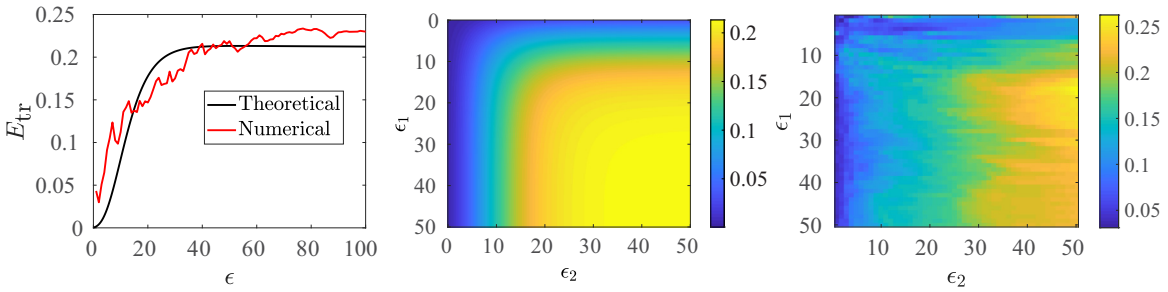

FIG. 8. Left panel: plot of the semianalytical approximation of $E_{\rm tr}(\epsilon)$ discussed in the context of Fig. 6 for $\epsilon_1 = \epsilon_2 = \epsilon$. Middle and right panels: plot of $E_{\rm tr}(\epsilon_1, \epsilon_2)$ compared with a zoomed in panel of Fig. 6. The middle panel is the analytical approximation while the right panel represents the numerics.

We now consider the case where $\epsilon_1 \neq \epsilon_2$ and minimize (11) using (12). The middle and right panels in Fig. 8 compare the crude theoretical approximation to the numerical findings. Given the reasonable qualitative agreement observed, this comparison suggests that the relevant estimation of the trapped fraction of the energy roughly captures the corresponding main contributions and yields a semianalytical handle of some usefulness.

Dynamical trapping of a solitary wave

In the same spirit as before (of trying to optimize the energy fraction trapped between the defects), one can envision dynamic protocols that enable capturing a traveling wave between two defects. As just a prototypical example of how to achieve this, we can consider a dynamic tuning of the resonator properties that can be performed as the system evolves. Since in realistic experiments changing the masses is difficult, we need to consider alternative ways to alter the local properties (and hence the reflection and transmission properties of the defects) on the fly. Motivated by the recently argued ability to dynamically (in time and/or space) tune elastic prefactors [21], we consider the possibility of modifying κ over time (i.e., the prefactor of the linear interaction of the woodpile with its internal resonator), e.g., in the form

$$\kappa(t) = k_1 + (k_2 - k_1)\frac{1 + \tanh\left(\frac{t-t_0}{\tau}\right)}{2}. \tag{13}$$

This functional form interpolates between k_1 and k_2, while if considering dynamics from $t = t_0$ onwards, the interpolation is between $\frac{1}{2}(k_1 + k_2)$ at $t = t_0$ and k_2 is the κ as $t \to \infty$. In order to thus dynamically trap the solitary wave we envision the following scenario. We allow the solitary wave to pass from the first (potential) defect at $d_1 = 0$ *without* having a defect in that location, i.e., effectively $\kappa(t) = 0$ there when the wave first passes; this way none of the wave's energy is reflected or transmitted during this first pass. Then, the wave arrives at $d_2 = 20$. In the latter location there is a "fixed" (not varying in time) defect with $\kappa = 2.5$. Notice that for both locations, we have selected a mass of $\epsilon_1 = \epsilon_2 = 10$. Once the wave arrives at $d_2 = 20$, we can observe in its dynamical evolution shown in Fig. 9 that it gets chiefly reflected.

During the time frame when the wave moves from $d_1 = 0$ to $d_2 = 20$, the dynamical defect at $d_1 = 0$ is put in place. In particular, we use Eq. (13) with $k_1 = 0$, $k_2 = 2.5$, $t_0 = 40$, $\tau = 0.1$, i.e., a defect with $\kappa = 2.5$ arises at this location within a short time frame around $t \approx 40$. Unfortunately, due to the traveling front nature of the wave, this causes a trapping and reflection at the location of the wave (observed in Fig. 9), however, this is mostly inconsequential in connection to the propagation of the wave. The most adverse side effect of this is that a small fraction of energy created by the "raising" of the defect at $d_1 = 0$ propagates inside the region between d_1 and d_2 and affects both (weakly) the motion of the wave and (also weakly but nontrivially) the amount of trapped energy in this region. Importantly, once this nontrivial defect at $d_1 = 0$ has been dynamically raised, it causes the wave to subsequently be chiefly reflected both at $d_1 = 0$ and at the fixed defect at $d_2 = 20$ with its energy remaining mainly trapped in the region between the two defects. This dynamical emergence of a defect clearly achieves the confinement of the wave's largest energy fraction within the desired region. One can naturally envision multiple alternative scenarios leading to such a confinement, yet we believe that this simple proof of principle illustrates the main idea and can motivate further studies along this vein.

V. CONCLUSIONS AND FUTURE CHALLENGES

In the present work, we have considered a nonlinear granular chain with multiple MwM defects that can be experimentally tested in some parameter regimes. Using a woodpile elastic lattice as our experimental motivation, we

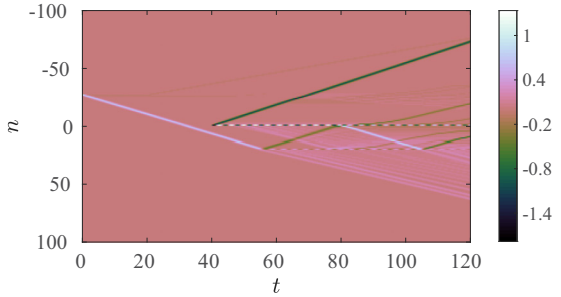

FIG. 9. Space-time velocity plot for the system with two defects of equal mass: $\epsilon_1 = \epsilon_2 = 10$. The first defect, at $d_1 = 0$, is dynamically switched on with $\kappa(t)$ given by (13), where $k_1 = 0$, $k_2 = 2.5$, $t_0 = 40$, $\tau = 0.1$. The second defect, at $d_2 = 20$, has fixed $\kappa = 2.5$. Observe that this setting achieves the trapping of a significant fraction of the solitary wave's energy, in the sense of it bouncing back and forth between the two defect sites.

illustrated how one can realize and probe such a system for the cases of one and two defects represented by longer rods in the orthogonally stacked chain. Laser Doppler vibrometry then enabled us to measure the (kinetic) energy transmitted, reflected and trapped at this "defective" region. We then turned to a series of theoretical and numerical considerations. We examined how trapped, transmitted and reflected energy fractions change as we vary the size of the region bearing the resonators. We considered the variation of the masses of the resonators and were able to numerically optimize the trapped region, as well as obtain a qualitative understanding of this optimization on the basis of transmissions and reflections of the principal traveling wave within the system. Finally, we proposed dynamical scenarios of variable elastic properties and utilized them to further enhance the potential of trapping energy within the region enclosed by our "defects."

This study opens numerous directions for the potential of directing and manipulating energy in such elastic woodpile lattices. The tunability of the rod lengths and possibly also of the elastic constants provides a large potential for considering defect regions of different sizes and properties in a highly tractable and controllable experimental setting. Extending such considerations to two-dimensional woodpile lattices and achieving the steering, and channeling of the energy in a controllable fashion, possibly reminiscent of analogous propositions in optics [22], may be of particular interest for future theoretical and experimental work.

We conclude by noting that, admittedly, the elastic woodpile lattices may be less straightforwardly amenable to some of the intriguing directions considered in the present study, such as examples of dynamic manipulation and their utilization for controllable energy trapping. However, we have become recently aware of an experimental realization of a different type of nonlinear mechanical lattice reported in [23]. Our direct interactions with the authors of this work suggest that not only is it possible to insert controllable defects in this setting, it has already been done in the preliminary studies recently presented [24]. Hence, we believe that such exciting directions may be explored in the imminent future.

ACKNOWLEDGMENTS

J.Y. and E.K. are grateful for the support from the National Science Foundation through Grant No. CAREER-1553202. E.K. acknowledges the support from the National Research Foundation of Korea (NRF) grant funded by the Korea government (MSPI, Grant No. 2017R1C1B5018136). J.Y. and P.G.K. also acknowledge the support from the ARO (Grant No. W911NF-15-1-0604) and AFOSR (FA9550-17-1-0114). P.G.K. acknowledges that this paper was made possible by NPRP Grant No. [8-764-1-160] from the Qatar National Research Fund (a member of Qatar Foundation). The findings achieved herein are solely the responsibility of the authors. P.G.K. also acknowledges support from the National Science Foundation under Grants No. DMS-1312856 and No. PHY-1602994, the Alexander von Humboldt Foundation, and the Stavros Niarchos Foundation via the Greek Diaspora Fellowship Program. He also acknowledges useful discussions with A. Vakakis. X.H. and S.H. gratefully acknowledge funding from the Department of Mathematics and Statistics (UMass) under the "Research Experience for Undergraduates" (REU) program. The work of A.V. was supported by the U.S. National Science Foundation through Grant No. DMS-1506904.

[1] V. F. Nesterenko, *Dynamics of Heterogeneous Materials* (Springer-Verlag, New York, 2001).
[2] S. Sen, J. Hong, J. Bang, E. Avalos, and R. Doney, Phys. Rep. **462**, 21 (2008).
[3] P. G. Kevrekidis, IMA J. Appl. Math. **76**, 389 (2011).
[4] G. Theocharis, N. Boechler, and C. Daraio, in *Phononic Crystals and Metamaterials* (Springer Verlag, New York, 2013), Chap. 6.
[5] M. A. Porter, P. G. Kevrekidis, and C. Daraio, Phys. Today **68**(11), 44 (2015).
[6] Yu. Starosvetsky, K. R. Jayaprakash, M. Arif Hasan, and A. F. Vakakis, *Topics on the Nonlinear Dynamics and Acoustics of Ordered Granular Media* (World Scientific, Singapore, 2017).
[7] C. Chong, M. A. Porter, P. G. Kevrekidis, and C. Daraio, J. Phys.: Condens. Matter **29**, 413003 (2017).
[8] X. Ni, P. Rizzo, J. Yang, D. Khatri, and C. Daraio, NDT&E International **52**, 76 (2012).
[9] A. Spadoni and C. Daraio, Proc. Natl. Acad. Sci. U.S.A. **107**, 7230 (2010).
[10] B. Liang, B. Yuan, and J. C. Cheng, Phys. Rev. Lett. **103**, 104301 (2009).
[11] X.-F. Li, X. Ni, L. Feng, M.-H. Lu, C. He, and Y.-F. Chen, Phys. Rev. Lett. **106**, 084301 (2011).
[12] N. Boechler, G. Theocharis, and C. Daraio, Nat. Mater. **10**, 665 (2011).
[13] F. Li, P. Anzel, J. Yang, P. G. Kevrekidis, and C. Daraio, Nat. Commun. **5**, 5311 (2014).
[14] C. Daraio, V. F. Nesterenko, E. B. Herbold, and S. Jin, Phys. Rev. E **72**, 016603 (2005).
[15] V. F. Nesterenko, C. Daraio, E. B. Herbold, and S. Jin, Phys. Rev. Lett. **95**, 158702 (2005).
[16] L. Bonanomi, G. Theocharis, and C. Daraio, Phys. Rev. E **91**, 033208 (2015).
[17] G. Gantzounis, M. Serra-Garcia, K. Homma, J. M. Mendoza, and C. Daraio, J. Appl. Phys. **114**, 093514 (2013).
[18] P. G. Kevrekidis, A. Vainchtein, M. S. Garcia, and C. Daraio, Phys. Rev. E **87**, 042911 (2013).
[19] E. Kim, F. Li, C. Chong, G. Theocharis, J. Yang, and P. G. Kevrekidis, Phys. Rev. Lett. **114**, 118002 (2015).
[20] E. Kim and J. Yang, J. Mech. Phys. Solids **71**, 33 (2014).
[21] F. Li, C. Chong, J. Yang, P. G. Kevrekidis, and C. Daraio, Phys. Rev. E **90**, 053201 (2014).
[22] D. N. Christodoulides and E. D. Eugenieva, Phys. Rev. Lett. **87**, 233901 (2001).
[23] Y. Watanabe, M. Nishimoto, and C. Shiogama, Nonlinear Theory Appl. IEICE **8**, 146 (2017).
[24] Presentation of Y. Watanabe in the Nonlinear Localization in Lattices (NLL 2018); (private communications).